# Efficiency of Multiexciton Generation in Colloidal Nanostructures

ANDREW SHABAEV,[†] C. STEPHEN HELLBERG,[‡] AND
ALEXANDER L. EFROS[*, †, ‡]

[†]*George Mason University, Virginia 22030, United States, and* [‡]*Naval Research
Laboratory, Washington, D.C. 20375, United States*

## CONSPECTUS

Solar energy production, one of the world's most important unsolved problems, has the potential to be a source of clean, renewable energy if scientists can find a way of generating cheap and efficient solar cells. Generation of multiple excitons from single photons is one way to increase the efficiency of solar energy collection, but the process suffers from low efficiency in bulk materials. An increase of multiexciton generation efficiency in nanocrystals was proposed by Nozik in 2002 and demonstrated by Schaller and Klimov in 2004 in PbSe nanocrystals. Since then, scientists have observed efficient multiexciton generation in nanostructures made of many semiconductors using various measurement techniques.

Although the experimental evidence of efficient carrier multiplication is overwhelming, there is no complete theory of this phenomenon. Researchers cannot develop such a theory without a self-consistent description of the Coulomb interaction and a knowledge of mechanisms of electron and hole thermalization in nanostructures. The full theoretical description requires the strength of the Coulomb interaction between exciton and multiexciton states and the thermalization rates, which both vary with the dimensionality of the confining potential. As a result, the efficiency of multiexciton generation depends strongly on the material and the shape of the nanostructure.

In this Account, we discuss the theoretical aspects of efficient carrier multiplication in nanostructures. The Coulomb interaction couples single excitons with multiexciton states. Phenomenological many-electron calculations of the evolution of single-photon excitations have shown that efficient multiexciton generation can exist only if the rate of the Coulomb mixing between photo-created exciton and biexciton states is significantly faster than the rate of exciton relaxation. Therefore, to increase multiexciton generation efficiency, we need to either increase the exciton-biexciton mixing rate or suppress the exciton relaxation rate. Following this simple recipe, we show that multiexciton generation efficiency should be higher in semiconductor nanorods and nanoplatelets, which have stronger exciton–biexciton coupling due to the enhancement of the Coulomb interaction through the surrounding medium.
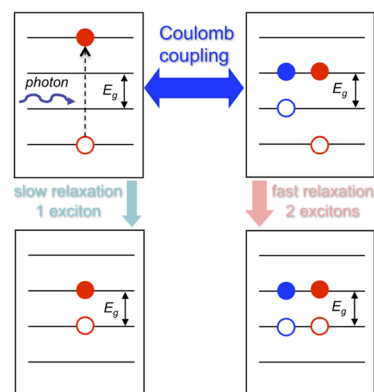
## 1. Introduction

Solar energy production has become one of the most important and challenging problems of our generation. Solar power can be an important source of clean, renewable energy if we can find ways to increase the efficiency of inexpensive solar cells. Conventional photovoltaic solar cells are based on the $p-n$ junction, which separates the newly created electron–hole ($e-h$) pair, allowing the energy to be extracted. The maximum energy collection efficiency of such a photovoltaic cell, in which each photon generates one $e-h$ pair, is the so-called Shockley–Queisser limit, approximately 32% percent.[1] Most of the solar photon energy absorbed by this device, including all of the photon energy in excess of the energy gap, is lost as heat. It is clear that if we could find a way to utilize this lost energy, we could greatly increase the efficiency of solar energy conversion.

Carrier multiplication is one way to boost the solar collection efficiency. If an optical excitation with energy, $\hbar\omega$, provides carriers an excess energy, $\hbar\omega - E_g$, which is greater than the semiconductor energy gap, $E_g$, these carriers can create a second $e-h$ pair via impact ionization of the filled band as shown in Figure 1a. Through this
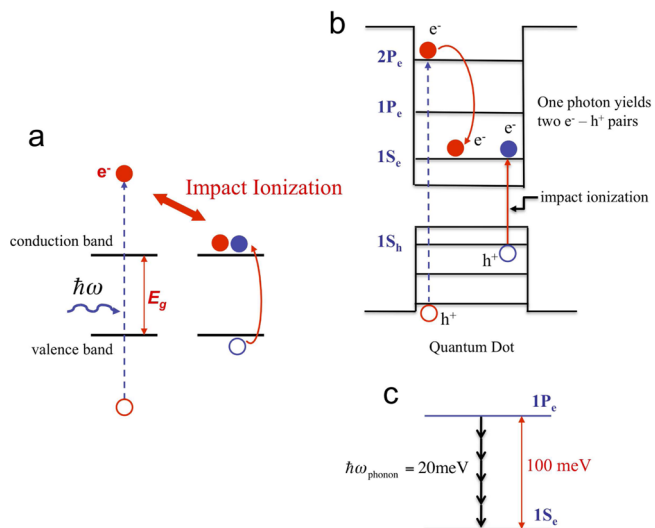
**FIGURE 1.** Carrier multiplication via impact ionization can be used to extract addition energy from high-energy photons by generating additional e−h pairs from highly excited carriers. (a) In bulk semiconductors, an energetic electron (or hole) decays to the band edge, exciting an additional electron and hole. The impact ionization rate in bulk materials is very small. (b) In nanocrystals, impact ionization is an inverse Auger process. Carriers decay from one discrete level to another, exciting addtional e−h pairs. The impact ionization rate in nanocrystals is significantly enhanced relative to the bulk. (From ref 2.) (c) The energy spacings between electron (and hole) levels in a nanocrystal are typically much larger than phonon energies, creating a "phonon bottleneck", inhibiting carrier relaxation.



**FIGURE 2.** Transient absorption measurements can be used to quantify the carrier density in a nanocrystal. (a) A high-energy photon absorbed by a NC can create either a single exciton or multiexciton state. The multiexciton state quickly relaxes to a single exciton, which then decays at a much slower rate. (b) Time-dependent absorption measurements of a probe photon at the ground state energy $E_g$ in PbSe NCs from ref 4. The high energy pump photon is absorbed at time $t = 0$. At lower pump photon energies, the probe absorption is nearly constant in time, indicating the presence of a single exciton. For energies above four times the energy gap in this case, multiexciton states are created which quickly decay to a single exciton. The multiplicity of the excitonic state can be estimated from the ratio of the absorption at short times to the absorption at longer times.

process, two e−h pairs can be collected instead of just one, significantly increasing the efficiency of solar cell energy conversion. Carrier multiplication is very inefficient in bulk semiconductors where carrier thermalization, which always competes with impact ionization, is much faster.

Arthur Nozik[2] first suggested that carrier multiplication in semiconductor nanocrystals (NCs) can be greatly enhanced. There are two reasons for this enhancement:

(1) Impact ionization, the creation of two electrons and one hole from one electron, is the inverse of the direct Auger process (see Figure 1b). It was shown theoretically and experimentally that the rate of direct Auger processes, during which two electrons and one hole create one excited electron, is strongly enhanced in NCs. This suggests that the same phenomenon occurs with the inverse Auger process because the rate of direct and inverse Auger processes is controlled by the same transition matrix element between a single-electron state and a state consisting of two electrons and one hole, commonly called a trion. The transition is caused by the multielectron Coulomb interaction $v(r_1, r_2)$ between charges. Figure 1b shows an example of the inverse Auger process in a PbSe NC. The transition takes place between the $|2P_e\rangle$ electron level and the $|1S_e 1S_e 1S_h\rangle$
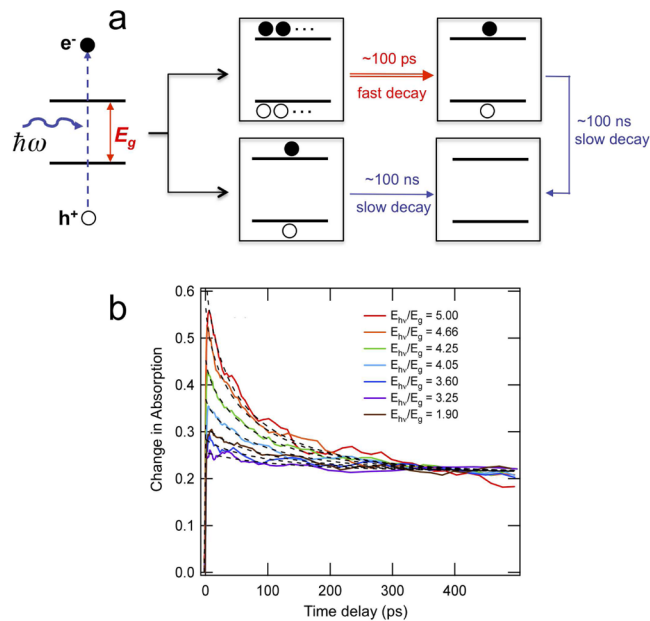
trion state, where the degenerate 1S electrons have opposite spins, and is described by the $\langle 2P_e|v(r_1, r_2)|1S_e 1S_e 1S_h\rangle$ matrix element.

(2) The rate of carrier thermalization is suppressed due to the discrete character of the electron−hole spectra. In PbSe nanocrystals, the electron- and hole-level spacings are much larger than the phonon energy, suppressing phonon assisted carrier thermalization as shown in Figure 1c. Direct carrier thermalization in this case should result from the simultaneous emission of many phonons, a process that has a small probability of occurring. This leads to the so-called "phonon bottleneck" for carrier relaxation; as a result, impact ionization may successfully compete with cooling.

## 2. Experimental Background

Indeed, soon after Nozik's publication, Schaller and Klimov[3] observed ultraefficient multiexciton generation (MEG) by a single photon in PbSe NCs using band-edge transient absorption measurements. The idea behind these measurements is depicted in Figure 2. The filling of the conduction
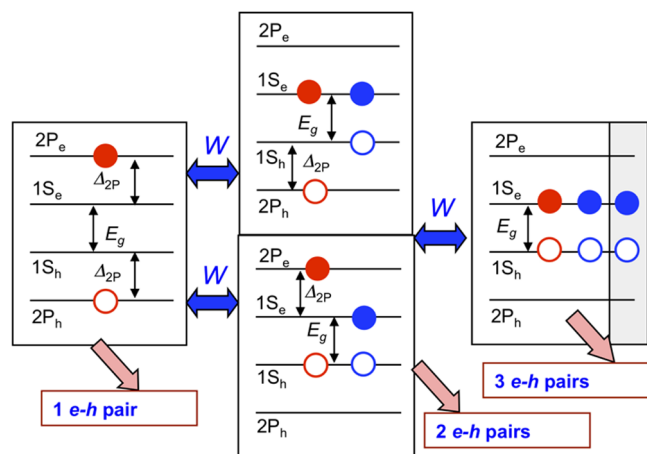
**FIGURE 3.** Resonant coherent superposition model of MEG in NCs. High energy exciton states (left panel) are coupled with multiexciton states through the Coulomb interaction, $W$, represented by the blue arrows. Pink arrows show thermalization to the ground state.[4]
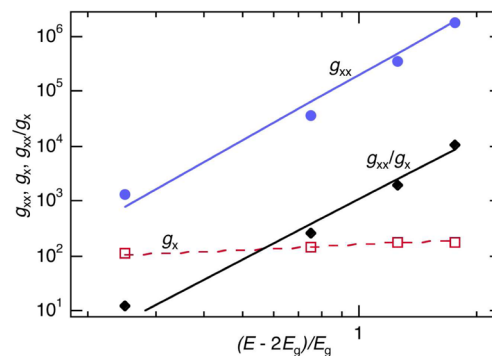


**FIGURE 4.** Calculated degeneracies of excitons (open red squares) and biexcitons (solid blue circles) as a function of energy. From ref 22. The solid black diamonds show the ratio of the biexciton to exciton degeneracies.

and valence band-edge states by photoexcited carriers decreases the absorption coefficient of a probe photon at the frequency of the ground state exciton of the NC. One can see that optical excitations with energy less than twice the energy gap (brown line in Figure 2b) create an almost time-independent induced absorption connected with one exciton. With increasing excitation frequency, one photon can generate a multiexciton. The fast decay of these excitons seen in the induced absorption during first 100 ps in Figure 2b is controlled by nonradiative Auger recombination. The magnitude of the change in absorption is approximately proportional to the relative filling factor $F$. In PbSe, which has four equivalent valleys in the conduction and valence bands, one can insert no more than eight electrons and eight holes in the lowest $1S_e$ and $1S_h$ levels, and the filling factor can be written as $F = (n_e + n_h)/8$, where the $n_e$ and $n_h$ are the number of electrons and holes in a NC, respectively, and $n_e \leq 8$ and $n_h \leq 8$. For a single exciton, $F = 1/4$. The change in absorption created by a single exciton in PbSe NCs can last for hundreds of nanoseconds, the time of the radiative exciton decay. In the case of two ground-state excitons, the filling factor is $F = 1/2$. The resulting time dependence of the change in absorption allows one to estimate the number of electron–hole pairs created by a single photon.[3]

Later, efficient MEG was observed by many groups using different techniques in NCs of many semiconductors: PbSe,[4−7] PbS,[4,8] Si,[9] CdSe,[10−12] InAs,[13,14] and in carbon nanotubes.[15] At the same time, some groups were not able to observe MEG in CdSe[16] and InAs[17,18] NCs and found the efficiency of MEG measured in PbSe NCs[7] was appreciably smaller than that reported earlier. The diverse experimental data on

MEG efficiency are now converging to more modest values for PbS and PbSe NCs.[19,20] But still the revised data for PbSe NCs has a quantum yield (QY) of carrier multiplication that reaches 250% (see, for example, Figure 1 from the Account by Padilha et al. in this issue.).[20]

## 3. Theoretical Background

Generally there are two models that explain the high efficiency of MEG in NCs. The first is the resonant coherent superposition model. Single electron and hole states are not eigenstates of a NC if the interparticle Coulomb interaction is included. The actual eigenstates are linear superpositions of carriers, trions, and higher order $e$–$h$ complexes. As a result, optical excitations create mixtures of excitons, biexcitons, triexcitons, and so forth, as shown in Figure 3. In the simplified version of this model,[4,21] the MEG efficiency is determined by the ratios of the exciton and biexciton relaxation rates and the rate of Coulomb mixing between exciton and biexciton states.

Noncoherent models for efficient MEG in NCs[23−26] are based on the important observation that the density of biexciton states is significantly larger than the density of exciton states at the same energy.[23] Figure 4 compares these densities in PbSe NCs.[22] The density of biexciton states is significantly larger than the density of excitons if the photon energy exceeds twice the energy gap. For such calculations it was shown that only the density of the trion states, which is also much larger than the density of exciton states, is important for efficient MEG.[27] The calculations of MEG efficiency in these noncoherent models are based on Fermi's Golden Rule, which requires that the final biexciton state decays much faster than rate of the exciton-biexciton transition, an assumption that has not been justified either experimentally or theoretically.
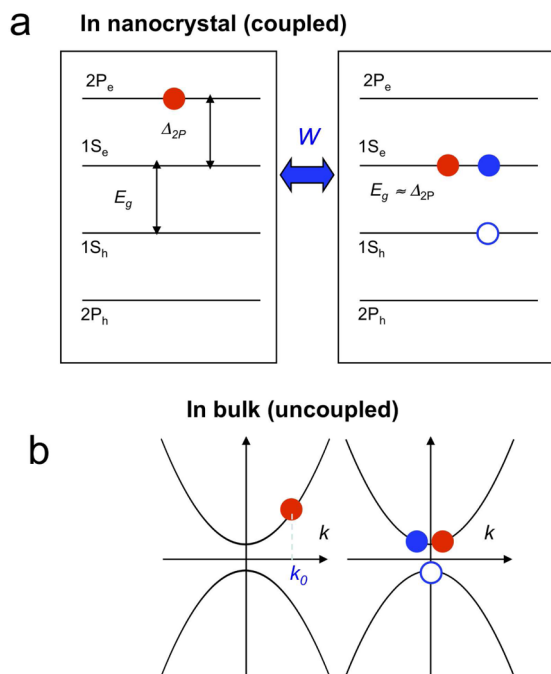
**FIGURE 5.** Degenerate single-electron and trion states. (a) In a NC, the states are coupled by the Coulomb interaction. (b) In the bulk, the degenerate single-electron and trion states have different total momenta and are not coupled.



**FIGURE 6.** Coherent superpositions of single electron and trion states. (a) Electron−hole configurations of the superpositions created by $2P_e$ (red) and $2D_e$ (blue) electrons in PbSe NCs. (b) Dependence of the energy on NC size of the $|2P_e\rangle$ electron and $|1S_e1S_e1S_h\rangle$ trion coupled states (red); and of the $|2D_e\rangle$ electron and $|1P_e1S_e1S_h\rangle$ trion coupled states (blue). In both cases, single electron and trion states are nearly degenerate over a wide range of NC diameters. Inset: Size dependence of the lowest single-particle electron and hole levels calculated in PbSe NCs. The trion states are grouped in boxes.

To explain the limitations of these two approaches, let us first consider the coherent superposition model. Consider a single electron occupying the $2P_e$ state of a spherical PbSe NC. The structure of the several lowest levels in such a NCs are shown schematically in Figure 5a. The energy gap of the NC, $E_g$, is the difference between the ground $1S_e$ electron and the ground $1S_e$ hole levels. Calculations of the size dependence of the lowest electron and hole levels within the effective mass model of Kang and Wise[28] show that, for a range of reasonable sizes, the energy difference between the $2P_e$ and the ground $1S_e$ electron levels ($\Delta_{2P}$) is very close to the effective energy gap, $E_g$. Thus, one electron in the $2P_e$ level is degenerate with the $|1S_e1S_e1S_h\rangle$ trion state, consisting of two $1S$ electrons (with opposite spins) and one $1S$ hole.

These states are coupled via multielectron Coulomb interactions:

$$W = \langle 2P_e|v(\mathbf{r}_1,\mathbf{r}_2)|1S_e1S_e1S_h\rangle \neq 0. \qquad (1)$$

The electron and the trion states are degenerate and coupled, and the NC eigenstates with energy $2P_e$ are linear superpositions of single electron and trion states. Consequently, the single-electron approximation is no longer a valid description of the $2P_e$ level. In general, the single-electron approximation breaks down for all
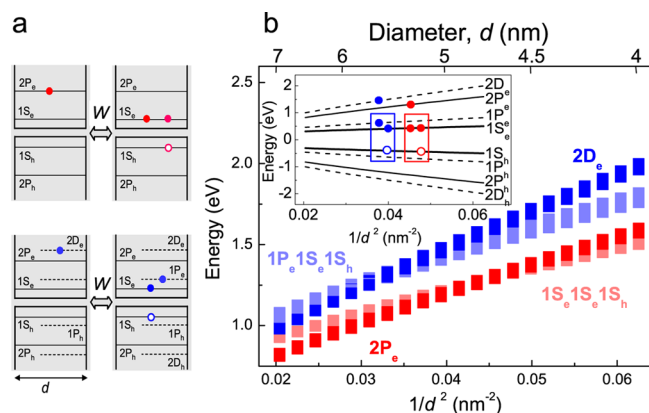
electron and hole states with energies greater than the energy gap.

This electron-trion coupling does not occur in bulk semiconductors because an electron with kinetic energy equal to the energy gap must have a very large momentum, while the trion has a much smaller momentum (see Figure 5b). The single-electron approximation in bulk is protected by the conservation of momentum.

In NCs, however, momentum is a bad quantum number, and the single-electron approximation for carriers with kinetic energy larger than the effective energy gap is not valid. The wave function of the so-called $2P_e$ electron state is a mixture of a single electron state and the trion $|1S_e1S_e1S_h\rangle$ state. Figure 6 shows the size dependence of the energy of the $2P_e$ electron state and the $|1S_e1S_e1S_h\rangle$ trion state, which allows us to identify the range of strongest coupling, where the energy difference of these two states is comparable to the strength of the coupling.

All higher electron levels also are coupled to various trion states. For example, the Coulomb interaction mixes the $2D_e$ electron state with a trion consisting of two electrons occupying the $1S_e$ and $1P_e$ levels and the hole in the $1S_h$ state. Calculations of the level structure shows the coupling between $2D_e$ and $|1P_e1S_e1S_h\rangle$ states is strong relative to their energy separation for a large range of the NC sizes. This observation reflects a general trend: the strong-coupling condition is much easier to realize for states with high energy.

The conduction and valence bands in PbSe are almost symmetrical; therefore, the $2P_h$ and $2D_h$ hole states also are strongly coupled with the respective trion states. In the strong coupling regime, the wave functions of conduction, $c$, and valence, $v$, band states are close to a 50%–50% mixture of single electron, $e$, or hole, $h$, states and the trion states:

$$\Psi_{2P}^{c,v} \approx \frac{1}{\sqrt{2}} (|2P_{e,h}\rangle + |1S_{e,h}1S_{e,h}1S_{h,e}\rangle),$$
$$\Psi_{2D}^{c,v} \approx \frac{1}{\sqrt{2}} (|2D_{e,h}\rangle + |1P_{e,h}1S_{e,h}1S_{h,w}\rangle) \tag{2}$$

What happens, however, if the strong coupling condition is not satisfied? The wave function of any electron or hole state in a NC is always a sum of single carrier, trion, and higher-order wave functions. This is true even when the confinement energy of electrons and holes $\Delta_{e,h}$ is smaller than the effective energy gap, $E_g$. In perturbation theory we have

$$\Psi_{nL}^c = \alpha_{nL}^c |nL_e\rangle + \sum_{k,l,m} \beta_{nL}^c(h,i,m)|kL_e^c iL_e^i mL_h^m\rangle,$$
$$\Psi_{nL}^v = \alpha_{nL}^v |nL_h\rangle + \sum_{k,l,m} \beta_{nL}^v(h,i,m)|kL_h^v iL_h^i mL_e^m\rangle \tag{3}$$

where $nL_e$ and $nL_h$ are the electron and hole states in spherical NCs, which are characterized by the spatial angular momentum $L = 0(S),1(P),2(D),3(F),...$ and main quantum numbers $n = 1,2,3...$ Generally the mixing coefficients $\beta$'s are very small if the strong coupling regime is not realized. On the other hand, the density of the trion states is very high. This raises the question of how a high density of weakly coupled states affects the coherent superposition model.'

All noncoherent models, which take into account the high density of the biexciton and trion states, describe the process of the biexciton creation using Fermi's Golden Rule. The probability of biexciton creation from a frequency $\omega$ exciton, $P_{\text{ex}\to\text{biex}}$, is described by

$$P_{\text{ex}\to\text{biex}} = \frac{2\pi}{\hbar} W_{e,b}^2 \rho_{\text{biex}}(\hbar\omega) \tag{4}$$

where $W_{e,b} = \langle\text{ex}|v(\boldsymbol{r}_1,\boldsymbol{r}_2)|\text{biex}\rangle$ is the Coulomb matrix element that describes the coupling between exciton and biexciton states, and $\rho_{\text{biex}}(\hbar\omega)$ is the density of biexciton states at the energy $\hbar\omega$. Equation 4, however, does not take into account the finite lifetime of the initial exciton and final states.

The finite lifetimes of these states can be taken into account within the density matrix approximation. The probability

of populating of the one $J$–biexciton state via its Coulomb coupling with the exciton state is described by the following expression:

$$P_{\text{ex}\to J\text{-biex}} = \frac{W_J^2(\gamma_1 + \gamma_2)}{(E_{\text{ex}} - E_J)^2/4 + W_J^2(1 + \gamma_1/\gamma_2) + \hbar^2(\gamma_1 + \gamma_2)^2} \tag{5}$$

where $E_{\text{ex}}$ and $E_J$ are the exciton and $J$-biexciton state energies, and $\gamma_1$ and $\gamma_2$ are the exciton and biexciton relaxation rates, respectively.[21] The total transition rate to the biexciton can be written as the sum over these events:

$$P_{\text{ex}\to\text{biex}} = \sum_J P_{\text{ex}\to J\text{-biex}} \tag{6}$$

In order to transform eq 6 to the expression of eq 4 given by Fermi's Golden Rule, we need to assume, first, that the biexciton decay rate is much faster than the biexciton creation rate and both of them are much larger than the exciton decay rate. In this approximation, eq 5 gives for the formation rate: $P_{\text{ex}\to J\text{-biex}} \approx W_J^2/\gamma_2\hbar^2$. Second, we need to assume that all Coupling matrix elements have the same value: $W^2 = \langle W_J^2\rangle$. Finally, the number of biexciton states where the exciton can transfer, $N_J$, should be estimated as the density of the biexciton state multiplied by the broadening connected with fast biexciton decay, $N_J = \rho_{\text{biex}}\hbar\gamma_2$. In this way, we arrive at eq 4.

The derivation of Fermi's Golden Rule from a more complex expression, which takes into account the relaxation rates of the initial and final states, requires some unphysical assumption about properties of excited states in NCs. If the first assumption of the derivation can be justified under some special conditions, the second approximation certainly is not valid in NCs, where the angular momentum is a reasonably good quantum number.

## 4. Unified Description for Symmetric Nanocrystals

A self-consistent model, which unifies both ideas and avoids all the above-mentioned approximations, was developed recently to describe efficient MEG in NCs.[29] The theory considers a single photon excitation coherently coupled with single and multiexciton states in a nanocrystal within the full quantum-state evolution approach. The time-dependent dynamic of the wave function of the modeled systems, $|\Psi(t)\rangle$, is described using a large, multiple-exciton basis,[29]

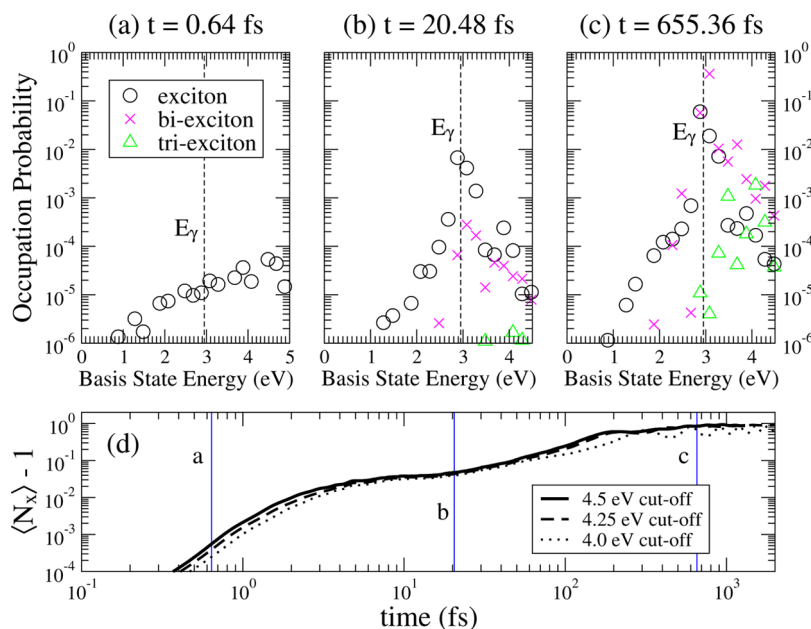$$\hbar\frac{d|\Psi(t)\rangle}{dt} = -i\hat{H}|\Psi(t)\rangle \tag{7}$$

**FIGURE 7.** Time dependent evolution of the $2P_e$–$2P_e$ excitation created by a single photon in a PbSe NC calculated for the closed-system Hamiltonian. The three upper panels (a–c) show the occupation probablities of exciton, biexciton, and triexciton states over 0.2 eV wide energy bins at three different snapshots in time. Panel (d) demonstrates convergence of the time dependence of the number of extra excitons $\langle N_x(t)\rangle - 1$ achieved by adjusting the energy cutoff of the included states. The vertical segments a–c show the time of snapshots, corresponding to the three upper panels.

The wave function $|\Psi(t)\rangle$ in eq 7 is linear superposition of hundreds of thousand of states, and the Hamiltonian $\hat{H}$ contains approximately $10 \times 10^7$ nonzero matrix elements. Following ref 29, let us consider first the evolution of the closed system, which conserves the photon energy and evolves only through the Coulomb interaction.

Figure 7 shows the time-dependent evolution of a $2P_e$–$2P_h$ excitation created by a single photon in a 2 nm radius PbSe NC at three snapshots in time.[29] The three upper panels (a), (b), and (c) show the occupation probability for exciton (circles), biexciton (crosses), and triexcitons (triangles) at $t = 0.64$, $20.48$, and $655.36$ fs, respectively. The occupation probabilities $\|\langle k|\Psi(t)\rangle\|^2$ are projections of the total wave function on the exciton ($k = 1$), biexciton ($k = 2$), and triexciton ($k = 3$) states. Panel (a) clearly demonstrates that it takes a time to create a biexciton. Biexcitons have been created by 20 fs as seen in panel (b). Comparison of panels (b) and (c) indicates that biexcitons have dominant contribution to the wave function by 1 ps time. Panel (d) shows the time dependence of the excess number of excitons. In small 2 nm radius NCs, a strong Coulomb coupling rapidly creates biexcitons with 90% probability if exciton and biexciton thermalization is ignored.

It is important to understand how the efficiency of MEG depends on the photon excitation energy. Figure 8a shows the formation of a multiexciton from a single photon
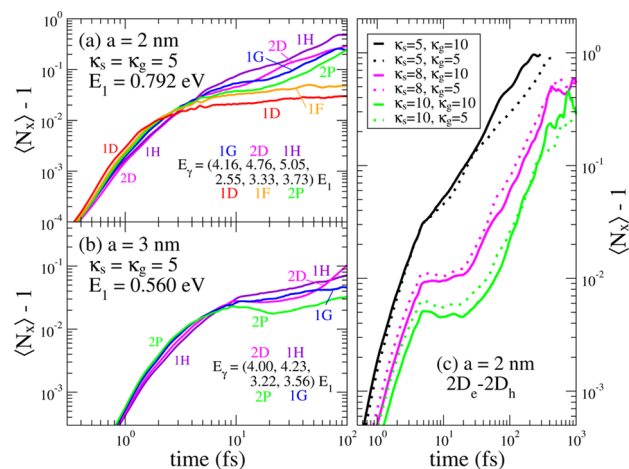


**FIGURE 8.** Evolution of the number of excitons $\langle N_x(t)\rangle$ created by a single-photon excitation at various optical transitions in PbSe NCs with radius $a = 2$ nm (a) and $a = 3$ nm (b). Energies are given in units of the effective energy gap. Panel (c) shows the time dependent evolution of $\langle N_x(t)\rangle$ created by a single-photon excitation of the $2D_e$–$2D_h$ transition in a 2 nm radius PbSe NC calculated for various combinations of the dielectric constants of the semiconductor nanocrystal $\kappa_s$ and the surrounding media $\kappa_g$.

excitation of different optically allowed transitions in 2 nm radius PbSe NCs.[29] In PbSe NCs such transitions occur between the electron and hole levels with the same angular momentum and the same main quantum numbers, such as $nL_e$–$nL_h$. One can see that the $2P_e$–$2P_h$ transition appears to provide the threshold for efficient MEG generation.
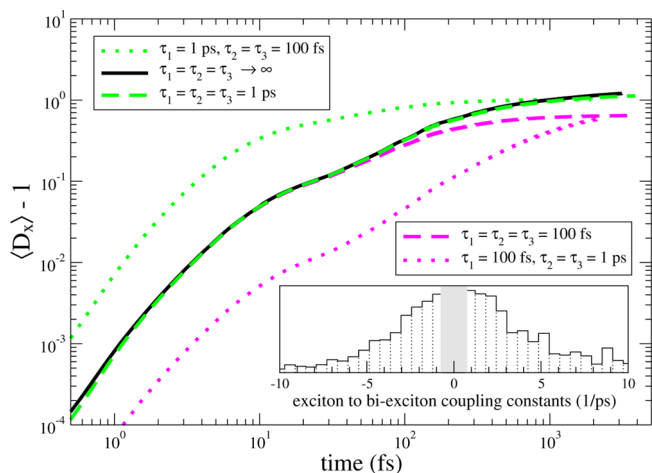
**FIGURE 9.** Average number of decayed-to-the-ground-state excitons $\langle D_x(t) \rangle$ for various combinations of relaxation times. The exciton, biexciton, and triexcition relaxation times are given by $\tau_1$, $\tau_2$, and $\tau_3$, respectively. A single-photon excitation of the $1H_e-1H_h$ transition of a PbSe NC with $a = 2$ nm radius NC is used. The inset shows the distribution of inverse coupling times between optically active exciton states and biexciton states, which are equal to the coupling Hamiltonian matrix elements, divided by $\hbar$. The inverse picosecond scale in the inset allows comparison of the typical coupling times with the thermalization times. The gray region is unresolved at our precision level and excluded from the distribution.

While the transitions with lower energies saturate around 10 fs to a very low probability of biexciton generation, the multiexciton probability continue to increase with time once the energetic threshold is reached. This is because the $2P_e$ and $2P_h$ levels are first states that are nearly degenerate with trion states.[4,21]

The strength of Coulomb interaction in the model[29] was controlled by the NC size and internal (semiconductor) and external (surrounding matrix) dielectric constants. A decrease of the Coulomb interaction strength through increasing the NC radius or dielectric constants significantly increases the time for MEG generation, as one can see in Figure 8b and c, respectively.

Note, that the time dependent evolution of the exciton population numbers does not show any coherent oscillations for the closed system considered, even in the case when MEG is efficient. The oscillations connected with the coherent superposition of exciton and biexciton states[4,21] are suppressed due to the large number of interacting biexciton states. The exciton becomes lost in the dense, multiexciton maze and does not appreciably revive.

This approach allows investigation of the effects of exciton and biexciton relaxation on the efficiency of MEG.[29] Figure 9 shows the effect of relaxation on the average number of ground-state excitons formed after a single photon excitation of the $1H_e-1H_h$ transition in 2 nm radius PbSe NCs. The excitation energy of this transition is equal to $5.05E_g$. The inset of Figure 9 shows the distribution of exciton−biexciton coupling strengths for this NC in units that allow one to compare these coupling strengths with the relaxation times of excitons and multiexcitons.

The solid black line in Figure 9 shows the time dependence of the number of excitons created by a single photon in the absence of all relaxation. The behavior is unchanged if the relaxation times of excitons and multiexcitons is 1 ps (green dashed line), which is obviously much slower than the $\approx$300 fs mixing time between excitons and biexcitons. Reduction of the biexciton and triexciton decay time to 100 fs (green dotted line) increases the rate of multiexciton formation in accordance with our previous considerations.[21] The saturation value of MEG depends strongly, however, on the ratio of $\tau_1$ to the Coulomb coupling strength. If the exciton relaxation time is 100 fs (dashed magenta line), MEG efficiency never reaches 200%. One sees that $\tau_2$ affects the rate of ME generation but does not affect the its efficiency. These calculations show that efficient MEG requires the exciton thermalization time to be longer than the exciton−biexciton coupling time.

## 5. Asymmetric Structures with Enhanced Coulomb Interactions

Anisotropic nanostructures, such as nanorods, nanoplatelets and nanowires, are surrounded by media with a small dielectric constant. Although electrons and holes are confined in the nanostructures, the electric field of their charge distribution is not confined within the nanostructures and penetrates into the surrounding medium. The dielectric constant of this medium is on the order of $\sim$2, which is usually significantly smaller than dielectric constant of the semiconductor, $\sim$23. The penetration of electric field into the surrounding media significantly enhances the strength of $e-h$ Coulomb interaction. Such enhancement, for example, increases dramatically of the exciton biding energy in such nanostructures. Calculations of PbSe nanowires and nanorods show that due to the small dielectric constant of the surrounding media, the exciton binding energy in a narrow nanowire can be as large as 400 meV.[30]

It is important to note that this enhancement is practically nonexistent in NCs because electron and hole charge distributions are almost identical in spherical NCs and compensate each other at each point of the NC. The NC retains its local neutrality even after exciton creation. This is not the case for nanorods, nanowires, and nanoplatelets, where the
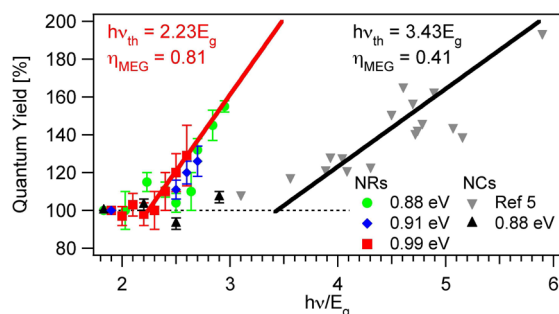
**FIGURE 10.** Comparison of MEG in PbSe nanorods and nanocrystals. Nanorods have a lower MEG threshold energy and a higher efficiency than nanocrystals. Reprinted with permission from ref 31. Copyright 2011 American Chemical Society.

electron−hole interaction at a distance is larger due to the small dielectric constant of the external media.

The enhancement of the Coulomb interaction in nanorods, nanowires, and nanoplatelets should increase MEG efficiency. The study of PbSe nanorods demonstrates enhancement of MEG relative to that measured in PbSe NCs.[31] Figure 10 shows the comparative measurements of MEG in PbSe nanorods and NCs with the band edges around 900 meV and 1 eV.[31] There is a significant increase in the MEG efficiency and a reduction in the MEG threshold to $2.23E_g$ in the nanorods. An MEG threshold equal to the energy conservation limit of twice the energy gap was reported in carbon nanotubes using a current measurement.[15] We believe that these significant improvements in MEG efficiency and decrease of the MEG threshold are connected with the enhancement of the Coulomb interaction and formation of the strongly bound excitons in these quasi one-dimensional structures.

# 6. Physics of Multiple Exciton Generation

Nanocrystals just a few nanometers in diameter require numerical methods that can handle very large numbers of atoms. Over last three decades, three theoretical approaches have been successfully used for calculations of the electronic structure in these large NCs: the multiband effective mass, tight binding, and semiempirical pseudopotential methods. Each method has its own advantages. The multiband effective mass method describes electronic spectra near a band edge very accurately. This approximation fails for higher levels with energies comparable to the energies of the higher bands. The tight binding and semiempirical pseudopotential methods, on the other hand, compute spectra over a wider range of energies by including more bands at the expense of accuracy at low energies.

All of these methods have been used to describe optically excited excitons. Description of MEG requires a Hilbert space consisting of excitons, biexcitons, triexcitons, etc. For example, an accurate basis for PbSe NCs contains over a hundred thousand states.[29] One also needs a self-consistent theory of the Coulomb coupling between excitons and multiexcitons, along with their electron−phonon coupling. Due to complexity of this problem, multiple approximations have to be used in practical solutions.[4,21,23−27,32] A self-consistent theory has been developed for very small crystals, such as $Si_{29}$ and $Ge_{29}$,[26,32] but has not yet been implemented for larger NCs.

Let us discuss the parameters which we use in our model calculations. The most important parameter is the matrix element that describes the coupling between an exciton and the asymmetric biexciton states (see Figure 2), where the Coulomb interparticle interaction was considered in the effective media model assuming a constant dielectric constant. Figure 11 shows the size-dependence of the matrix elements, $W = \langle 2P_e | v(\mathbf{r}_1, \mathbf{r}_2) | 1S_e 1S_e 1S_h \rangle$ and $W = \langle 2D_e | v(\mathbf{r}_1, \mathbf{r}_2) | 1P_e 1S_e 1S_h \rangle$ using the high frequency dielectric constant of bulk PbSe $\kappa_s = \kappa_g = 23$. One can see that the matrix elements increase superlinearly as a function of inverse NC radius. Calculations show also that this matrix element is larger for $2D_e−2D_h$ excitations.

However, what is the dielectric constant of a NC? One thing is clear: it is a high-frequency dielectric constant. Phonons do not contribute to the charge screening because the typical frequencies of carrier motion is much larger than phonon frequencies. It is known, that in narrow gap bulk semiconductors, such as PbSe, the high-frequency dielectric constant is inversely proportional to the semiconductor energy gap. What should happen to the dielectric constant of bulk PbSe ($\kappa = 23$) in PbSe NCs where the effective energy gap increases up to three times its bulk value of $E_g = 0.28$ eV (at $T = 300$ K) with decreasing radius? The decrease of the NC radius should strongly affect NC polarizability. Finally, due to the discrete character of the electron−hole energy spectrum, different multibody configurations play a role in the Coulomb potential screening for the various effects and processes we are studying. As a result, the matrix elements shown in Figure 11 should be considered only as estimates of the coupling strengths.

Unfortunately, after almost 30 years of research, we still lack a reliable description of the major mechanisms of the carrier thermalization in NCs. The major problem is we do not know how carriers overcome phonon bottleneck during their relaxation. The simultaneous emission of many phonons required for such a process is inconsistent with the fast thermalization time, which is on the order of 1−6 ps.[33]
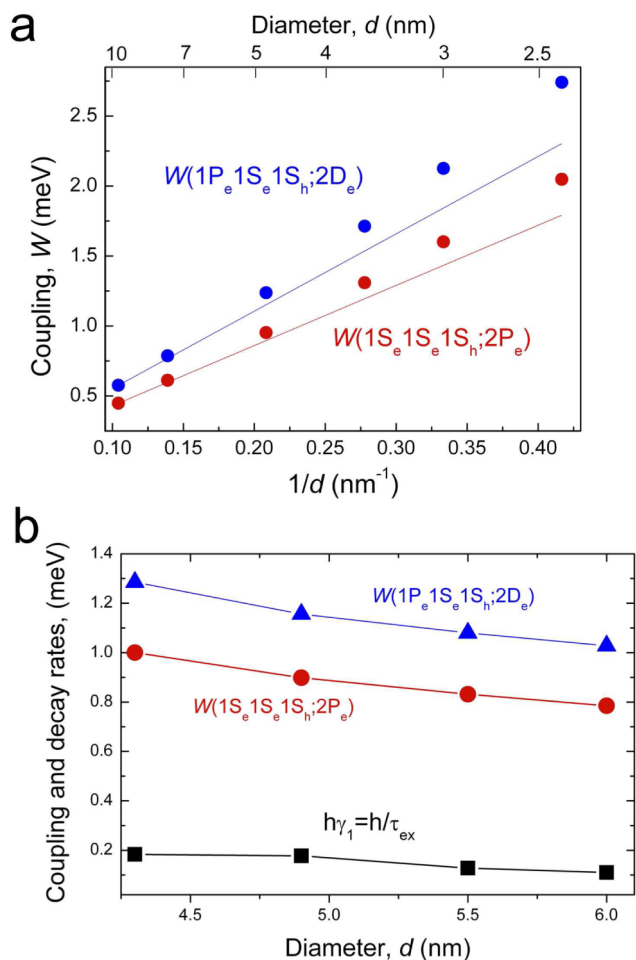
**FIGURE 11.** Coulomb coupling and exciton decay rates. (a) Dependence of the Coulomb matrix element, $W$, that describes coupling between two pairs of states: $|2P_e\rangle$ and $|1S_e1S_e1S_h\rangle$ (red points), and $|2D_e\rangle$ and $|1P_e1S_e1S_h\rangle$ (blue points) on the inverse of the NC diameter $d$. The straight solid lines show the asymptotic behavior at large $d$. Reprinted with permission ref 21. Copyright 2006 American Chemical Society. (b) Comparison of coupling strengths and exciton decay rates. Lines are guides for the eye.

Preliminary data also suggest that this relaxation could occur via emission of phonons from organic molecules at the NC's surface.[34]

Although the mechanism of the carrier thermalization is not established, we can assume that the relaxation rate is controlled by the strength of the phonon coupling with multi-$e$–$h$ configurations that would allows us to estimate the ratio of the exciton and biexciton relaxation rates. Our calculations indeed show that polar interactions of intrinsic semiconductor phonons in CdSe and PbSe NCs with asymmetric $e$–$h$ pair configurations are 10–20 times stronger than their coupling with the symmetric electron–hole pair configurations created by light. The charge distributions of the optically created electron and hole compensate each other almost exactly at each point of the nanocrystal, and the nanocrystal thus retains its local neutrality even after exciton creation.[35] As a result, the interactions between exciton and polar optical phonons are very weak. It also is quite obvious that the coupling of asymmetric $e$–$h$ configurations with phonons of organic molecules at the nanocrystal surface should be significantly stronger. If we assume that the relaxation rates for these configurations is proportional to this coupling, we see that $\gamma_2 \gg \gamma_1$. As shown above, the fulfillment of this condition should expedite the creation of multiexcitons.

Finally, can the model predict the efficient MEG observed in PbSe NCs? According to the model, efficient MEG can occur only if the exciton-to-biexciton coupling rate is larger than the exciton thermalization rate. We cannot calculate $\gamma_1$, but the measurements conducted in PbSe provide us the size dependence of the exciton thermalization time.[33] Comparing the size dependence of $\gamma_1$ with the size dependence of the coupling rate calculated for the bulk high frequency dielectric constant $\kappa = 23$, we see that this condition is fulfilled even for the lowest estimate of the coupling rate (see Figure 11b). In NCs, the effective dielectric constant is smaller than in the bulk. It is interesting to note that efficiency of MEG is inversely proportional to exciton thermalization rate, as shown in Figure 4 from ref 20. The comparison of MEG efficiency measured in PbS, PbSe, and PbTe NCs conducted in ref 20 shows that bulk optical phonons are responsible for the carrier thermalization in these NCs.

## 7. Summary

Our calculations unambiguously demonstrate that efficient multiexciton generation requires (1) strong Coulomb interactions between exciton and biexciton states and (2) suppression of the exciton thermalization time. In NCs, this enhancement can be reached only by decreasing the NC size. The Coulomb interaction should be significantly enhanced in colloidal nanorods, nanowires, and nanoplatelets due to the small dielectric constant of the surrounding media. This enhancement indeed leads to more efficient MEG as was recently demonstrated in PbSe nanorods and single-wall carbon nanotubes.

## BIOGRAPHICAL INFORMATION

**Andrew Shabaev** is a Research Assistant Professor at George Mason University. His research interests include electronic, magnetic and vibrational properties of bulk materials and nanometer-sized structures and their response in electromagnetic fields; pump−probe techniques for optical read-out and control of nanostructures; and applied projects in computational materials science.

**C. Stephen Hellberg** is a research physicist in the Center for Computational Materials Science at NRL where his work includes quantum dots and the properties of surfaces and interfaces. He received a Ph.D. from the University of Pennsylvania in 1993. After a postdoctoral appointment at Florida State University from 1993 to 1996, he moved to NRL, first as a postdoctoral fellow.

**Alexander L. Efros** received a PhD from St. Petersburg Technical University in 1978. From 1981 to 1990 he was a senior researcher at the Ioffe Institute, Leningrad. From 1990 to 1992 he was a senior researcher at the Technical University of Munich, and from 1992-1993 he was a visiting scientist at MIT. He moved to the Naval Research Laboratory in 1993. His pioneering work on electronic and optical properties of nanocrystal quantum dots was published in 1982. His research interest is in optical, transport, and magnetic properties of nanoscale semiconductor structures.

## FOOTNOTES

*To whom correspondence should be addressed. E-mail: efros@nrl.navy.mil.
The authors declare no competing financial interest.

## REFERENCES

1 Shockley, W.; Queisser, H. J. Detailed balance limit of efficiency of p-n junction solar cells. *J. Appl. Phys.* **1961**, *32*, 510–519.

2 Nozik, A. J. Quantum dot solar cells. *Phys. E* **2002**, *14*, 115–120.

3 Schaller, R. D.; Klimov, V. I. High Efficiency Carrier Multiplication in PbSe Nanocrystals: Implications for Solar Energy Conversion. *Phys. Rev. Lett.* **2004**, *92*, 186601.

4 Ellingson, R. J.; Beard, M. C.; Johnson, J. C.; Yu, P.; Micic, O. I.; Nozik, A. J.; Shabaev, A.; Efros, A. L. Highly Efficient Multiple Exciton Generation in Colloidal PbSe and PbS Quantum Dots. *Nano Lett.* **2005**, *5*, 865–871.

5 Trinh, M. T.; Houtepen, A. J.; Schins, J. M.; Hanrath, T.; Piris, J.; Knulst, W.; Goossens, A. P. L. M.; Siebbeles, L. D. A. In Spite of Recent Doubts Carrier Multiplication Does Occur in PbSe Nanocrystals. *Nano Lett.* **2008**, *8*, 1713–1718.

6 Ji, M.; Park, S.; Connor, S. T.; Mokari, T.; Cui, Y.; Gaffney, K. J. Efficient Multiple Exciton Generation Observed in Colloidal PbSe Quantum Dots with Temporally and Spectrally Resolved Intraband Excitation. *Nano Lett.* **2009**, *9*, 1217–1222.

7 Nair, G.; Geyer, S.; Chang, L.-Y.; Bawendi, M. Carrier multiplication yields in PbS and PbSe nanocrystals measured by transient photoluminescence. *Phys. Rev. B* **2008**, *78*, 125325.

8 Schaller, R. D.; Sykora, M.; Pietryga, J. M.; Klimov, V. I. Seven Excitons at a Cost of One: Redefining the Limits for Conversion Efficiency of Photons into Charge Carriers. *Nano Lett.* **2006**, *6*, 424–429.

9 Beard, M. C.; Knutsen, K. P.; Yu, P.; Luther, J. M.; Song, Q.; Metzger, W. K.; Ellingson, R. J.; Nozik, A. J. Multiple Exciton Generation in Colloidal Silicon Nanocrystals. *Nano Lett.* **2007**, *7*, 2506–2512.

10 Schaller, R. D.; Petruska, M. A.; Klimov, V. I. Effect of electronic structure on carrier multiplication efficiency: Comparative study of PbSe and CdSe nanocrystals. *Appl. Phys. Lett.* **2005**, *87*, 253102.

11 Schaller, R. D.; Sykora, M.; Jeong, S.; Klimov, V. I. High-Efficiency Carrier Multiplication and Ultrafast Charge Separation in Semiconductor Nanocrystals Studied via Time-Resolved Photoluminescence. *J. Phys. Chem. B* **2006**, *110*, 25332–25338.

12 Gachet, D.; Avidan, A.; Pinkas, I.; Oron, D. An Upper Bound to Carrier Multiplication Efficiency in Type II Colloidal Quantum Dots. *Nano Lett.* **2010**, *10*, 164–170.

13 Schaller, R. D.; Pietryga, J. M.; Klimov, V. I. Carrier Multiplication in InAs Nanocrystal Quantum Dots with an Onset Defined by the Energy Conservation Limit. *Nano Lett.* **2007**, *7*, 3469–3476.

14 Pijpers, J. J. H.; Hendry, E.; Milder, M. T. W.; Fanciulli, R.; Savolainen, J.; Herek, J. L.; Vanmaekelbergh, D.; Ruhman, S.; Mocatta, D.; Oron, D.; Aharoni, A.; Banin, U.; Bonn, M. Carrier Multiplication and Its Reduction by Photodoping in Colloidal InAs Quantum Dots. *Nature* **2007**, *111*, 4146–4152.

15 Gabor, N. M.; Zhong, Z.; Bosnick, K.; Park, J.; McEuen, P. L. Extremely Efficient Multiple Electron-Hole Pair Generation in Carbon Nanotube Photodiodes. *Science (New York, NY)* **2009**, *325*, 1367–1371.

16 Nair, G.; Bawendi, M. Carrier multiplication yields of CdSe and CdTe nanocrystals by transient photoluminescence spectroscopy. *Phys. Rev. B* **2007**, *76*, 081304.

17 Pijpers, J. J. H.; Hendry, E.; Milder, M. T. W.; Fanciulli, R.; Savolainen, J.; Herek, J. L.; Vanmaekelbergh, D.; Ruhman, S.; Mocatta, D.; Oron, D.; Aharoni, A.; Banin, U.; Bonn, M. Carrier Multiplication and Its Reduction by Photodoping in Colloidal InAs Quantum Dots. *Nature* **2008**, *112*, 4783–4784.

18 Ben-Lulu, M.; Mocatta, D.; Bonn, M.; Banin, U.; Ruhman, S. On the Absence of Detectable Carrier Multiplication in a Transient Absorption Study of InAs/CdSe/ZnSe Core/Shell1/Shell2 Quantum Dots. *Nano Lett.* **2008**, *8*, 1207–1211.

19 McGuire, J. A.; Joo, J.; Pietryga, J. M.; Schaller, R. D.; Klimov, V. I. New Aspects of Carrier Multiplication in Semiconductor Nanocrystals. *Acc. Chem. Res.* **2008**, *41*, 1810–1819.

20 Padilha, L. A.; Stewart, J. T.; Sandberg, R. L.; Bae, W. K.; Koh, W. K.; Pietryga, J. M.; Klimov, V. I. Carrier Multiplication in Semiconductor Nanocrystals: Influence of Size, Shape and Composition; chapter published in this volume. *Acc. Chem. Res.* 2013, in press, DOI: 10.1021/ar300228x.

21 Shabaev, A.; Efros, A. L.; Nozik, A. J. Multiexciton Generation by a Single Photon in Nanocrystals. *Nano Lett.* **2006**, *6*, 2856–2863.

22 Rupasov, V. I.; Klimov, V. I. Carrier multiplication in semiconductor nanocrystals via intraband optical transitions involving virtual biexciton states. *Phys. Rev. B* **2007**, *76*, 125321.

23 Schaller, R. D.; Agranovich, V. M.; Klimov, V. I. High-efficiency carrier multiplication through direct photogeneration of multi-excitons via virtual single-exciton states. *Nat. Phys.* **2005**, *1*, 189–194.

24 Allan, G.; Delerue, C. Role of impact ionization in multiple exciton generation in PbSe nanocrystals. *Phys. Rev. B* **2006**, *73*, 205423.

25 Franceschetti, A.; An, J. M.; Zunger, A. Impact Ionization Can Explain Carrier Multiplication in PbSe Quantum Dots. *Nano Lett.* **2006**, *6*, 2191–2195.

26 Hyeon-Deuk, K.; Prezhdo, O. V. Time-Domain ab Initio Study of Auger and Phonon-Assisted Auger Processes in a Semiconductor Quantum Dot. *Nano Lett.* **2011**, *11*, 1845–1850.

27 Rabani, E.; Baer, R. Distribution of Multiexciton Generation Rates in CdSe and InAs Nanocrystals. *Nano Lett.* **2008**, *8*, 4488–4495.

28 Kang, I.; Wise, F. W. Electronic structure and optical properties of PbS and PbSe quantum dots. *J. Opt. Soc. Am. B* **1997**, *14*, 1632–1646.

29 Witzel, W. M.; Shabaev, A.; Hellberg, C. S.; Jacobs, V. L.; Efros, A. L. Quantum Simulation of Multiple-Exciton Generation in a Nanocrystal by a Single Photon. *Phys. Rev. Lett.* **2010**, *105*, 137401.

30 Bartnik, A.; Efros, A.; Koh, W. K.; Murray, C.; Wise, F. Electronic states and optical properties of PbSe nanorods and nanowires. *Phys. Rev. B* **2010**, *82*, 195313.

31 Cunningham, P. D.; Boercker, J. E.; Foos, E. E.; Lumb, M. P.; Smith, A. R.; Tischler, J. G.; Melinger, J. S. Enhanced Multiple Exciton Generation in Quasi-One-Dimensional Semiconductors. *Nano Lett.* **2011**, *11*, 3476–3481.

32 Madrid, A. B.; Hyeon-Deuk, K.; Habenicht, B. F.; Prezhdo, O. V. Phonon-Induced Dephasing of Excitons in Semiconductor Quantum Dots: Multiple Exciton Generation, Fission, and Luminescence. *ACS Nano* **2009**, *3*, 2487–2494.

33 Harbold, J.; Du, H.; Krauss, T.; Cho, K.-S.; Murray, C.; Wise, F. Time-resolved intraband relaxation of strongly confined electrons and holes in colloidal PbSe nanocrystals. *Phys. Rev. B* **2005**, *72*, 195312.

34 Guyot-Sionnest, P.; Wehrenberg, B.; Yu, D. Intraband relaxation in CdSe nanocrystals and the strong influence of the surface ligands. *J. Chem. Phys.* **2005**, *123*, 074709.

35 Schmitt-Rink, S.; Miller, D.; Chemla, D. Theory of the linear and nonlinear optical properties of semiconductor microcrystallites. *Phys. Rev. B* **1987**, *35*, 8113–8125.